

Article

Antagonistic Magneto-Rheological Actuators with Inherent Output Boundedness: An Ideal Solution for High-Performance and Human-Safe Actuation

Mehrdad R. Kermani ^{*}, Sergey Pisetskiy, Ilia Polushin and Zi-Qi Yang 

Department of Electrical and Computer Engineering, Western University, London, ON N6A 5B9, Canada

^{*} Correspondence: mkermani@eng.uwo.ca

Abstract: This paper studies the working principles of antagonistic magneto-rheological (MR) actuators, i.e., a combination of an electric motor and a pair of MR clutches in an antagonistic configuration, for compliant actuation in robotics. The study focuses on the unique boundedness property exhibited by MR actuators, which limits the output torques delivered to the load, independent of the received input torque and/or control commands. This inherent property is of significant importance for ensuring human safety in human–robot interaction applications. Through a comprehensive analysis, we provide analytical proof of the inherent output boundedness of antagonistic MR actuators and validate our findings through experimental results. Our research demonstrates that these actuators are well-suited for safe operations in robotic applications, eliminating the need for additional sensor measurements or complex control strategies. This promising capability enables the avoidance of trade-offs between actuator performance, complexity, and cost. The insights gained from this study contribute to advancing compliant actuation technology, paving the way for high-performance and human-safe robotic systems.

Keywords: magnetorheological clutch; antagonistic actuator; compliant actuation; input-to-state stability; backdrivable; output boundedness



Citation: Kermani, M.R.; Pisetskiy, S.; Polushin, I.; Yang, Z.-Q. Antagonistic Magneto-Rheological Actuators with Inherent Output Boundedness: An Ideal Solution for High-Performance and Human-Safe Actuation.

Actuators **2023**, *12*, 351. <https://doi.org/10.3390/act12090351>

Academic Editors: Tao Chen, Minglu Zhu and Haidong He

Received: 3 August 2023

Revised: 21 August 2023

Accepted: 25 August 2023

Published: 31 August 2023



Copyright: © 2023 by the authors. Licensee MDPI, Basel, Switzerland. This article is an open access article distributed under the terms and conditions of the Creative Commons Attribution (CC BY) license (<https://creativecommons.org/licenses/by/4.0/>).

1. Introduction

The pursuit of high-performance compliant actuators is crucial for ensuring both the safety and effectiveness of collaborative robots [1]. However, achieving a balance between safe operation, high performance (i.e., torque, speed, repeatability), and affordability remains a challenge in the field of compliant actuation, since there is a significant difference in the performance and cost of compliant actuators depending on the technology they are built on. This paper aims to address this challenge by investigating a unique property of MR (magneto-rheological) actuators—their inherent output boundedness. Unlike conventional actuation methods, MR actuators possess a unique ability to limit their output speed and/or torque, irrespective of the input torque and control commands across the entire control bandwidth. This inherent boundedness, in conjunction with other advantageous characteristics such as precise torque control, broad bandwidth, and compliance [2], positions MR actuators as potential solutions to bridge the existing research gap in compliant actuator design. By studying this phenomenon in MR actuators, this study aims to achieve safe operation with high performance while maintaining cost effectiveness [3].

To better understand this gap, it is important to note two contrasting approaches in the design of compliant actuators. One common approach involves mimicking compliance behavior by controlling high-end actuators such as harmonic drive actuators solely based on sensor readings. Examples of robots using this approach include Franka, UR5/10/15, JACO, KUKA iiwa, and ABB YuMi [4–8]. These robots are designed with relatively small payloads and lightweight structures to ensure safe operation. These robots are more expensive to produce due to specific actuators and the sensors they require. However,

in recent years, there has been a large decrease in prices as collaborative robot development has gained momentum.

On the other end of the design spectrum are low-cost compliant actuators, primarily realized with series elastics or variable impedance components. Examples of robots using such actuators are Sawyer/Swayer Black Edition, its predecessor Baxter (now obsolete), and Spot Arm [9,10]. Although these robots are compliant, they have poor repeatability and cannot perform high-precision tasks. There have been some attempts at recuperating the actuation performance at the expense of increased design complexity, blurring the distinction between different types of collaborative robots.

Regardless of their actuation technology, all existing collaborative robots have limited torque capacity to ensure their safety, highlighting the existing technology gap. To the best of our knowledge, there is currently no compliant actuator that can simultaneously deliver very high torque while meeting the requirements of safe actuation and inherent compliance.

With this specific gap in mind, we previously developed a new compliant actuation paradigm using MR clutches. In this paradigm, each rotational axis of motion is driven by a pair of antagonistic MR clutches—one providing clockwise (CW) motion or torque and the other providing counterclockwise (CCW) motion or torque. All pairs of MR clutches are connected to a common active source, such as an electric motor. The actuation paradigm is depicted schematically in Figure 1.

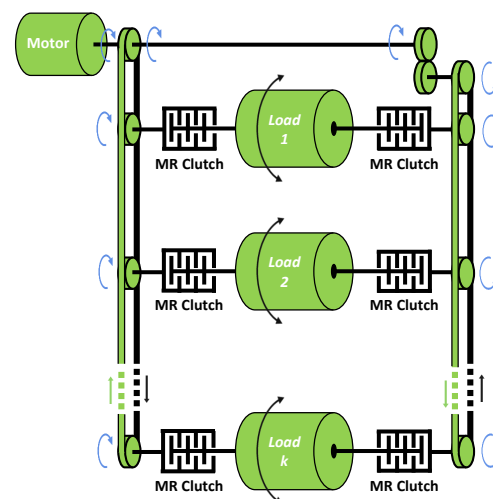


Figure 1. Multi-axis actuation paradigm using antagonistic MR clutches.

This actuation paradigm inherits all properties of MR clutches, including precise torque control, broad bandwidth, and inherent compliance [2,11]. This study extends these properties to include the inherent boundedness of the MR actuator output, highlighting its safe operation. Although an MR clutch is a passive device, one cannot claim such property is preserved in an MR actuator (i.e., a combination of an active source and MR clutches). We analytically study this problem, present theoretical proof, and experimentally show that this passive behavior is preserved in MR actuators, regardless of the closed-loop control commands and/or mechanical input to the MR clutches. It is shown that an MR actuator slows down the actuation speed as soon as its output speed exceeds a predetermined value. This behavior is not a response to any speed measurements and/or control actions, but rather an inherent behavior of the actuator. This behavior also extends to multi-axis actuation.

The inherent boundedness of the output of MR actuators, coupled with their low inertia, wide control bandwidth, precise torque control, and manufacturing simplicity, makes MR actuators a suitable solution for achieving safe, high-performance, and cost-effective actuation. Previous studies have focused on mechanical design [12] and/or characterization of MR fluids in MR clutches. This work, however, concentrates on the control of MR actua-

tors and represents the first study on the dynamic behavior of antagonistic MR actuators concerning the boundedness of their output. The findings of this study can serve as a basis for designing specific control strategies that comply with ISO/TS 15066 standards [13]. We validate the results using a one-joint mechanism, but they can be extrapolated to an n -DOF (degrees of freedom) manipulator with n pairs of antagonistic MR clutches. Discussions on an n -DOF system will be addressed in future publications.

The contributions of the work are as follows:

- In-depth analyses of output boundedness of antagonistic MR actuators.
- Theoretical investigation of global output boundedness of antagonistic MR actuators.
- Design of control algorithms specific to MR actuators for safe operation compliant with ISO/TS 15066 standards.
- Experimental studies to demonstrate and validate the output boundedness behavior.
- Exploration of MR actuators as potential solutions to bridge the research gap in compliant actuator design.

The organization of the paper is as follows: In Section 2, conventional antagonistic actuation and compliant actuation are briefly reviewed; Section 3 briefly explains the basics of an MR clutch and the principles of the antagonistic MR actuation; Section 4 is dedicated to analytical studies of the behavior of a pair of antagonistic MR clutches using a single joint mechanism; Section 5 demonstrates the behavior of antagonistic MR actuators experimentally and validates our theoretical analysis for global boundedness of the antagonistic MR actuator outputs; finally, Section 6 summarizes and concludes the paper.

2. Antagonistic Configuration and Compliance

Antagonistic actuation is a well-known and widely used approach with several realizations [14–16]. Regardless of the embodiment of the design, an antagonistic actuation requires compliant (backdrivable) actuators or compliant elements. The reason is somewhat obvious; when one actuator generates motion in the required direction, the other compliant actuator should not pose significant resistance to the motion. There is, however, a trade-off. A compliant actuator often results in degraded dynamic performance [14]. This loss of performance is the price of reducing or in some cases eliminating the reflected inertia of the actuator. Different technologies for realizing compliant actuators have been reported in the literature. For a recent survey of compliant actuators, see [3].

Compliant actuators built using artificial muscles such as super-coiled polymers [17,18] and shape memory alloys [19] have relatively large response time and are not able to perform fast motions.

Pneumatic actuators are fast, lightweight, and powerful. However, these actuators cannot ensure position accuracy and require a sophisticated control system to dampen unwanted oscillations of the actuated load [20].

Series Elastic Actuators (SEA) [21] use an elastic component embedded between the non-compliant drive mechanism and the load. Although this approach lowers the total impedance of the drive mechanism (i.e., motor and gearbox), the use of an elastic element limits the overall control bandwidth of the actuator, and undesired oscillations lead to control challenges.

More advanced solutions with variable compliance [22–26] further improve the performance of the actuators. Nevertheless, the limited bandwidth of the system as well as the complexity of the design still leads to limitations in the applicability of such actuators. The use of SEAs and variable compliance devices in antagonistic configuration brings additional challenges in terms of control since it is necessary to use and control more than one component for each axis of rotation [27–29].

In recent years, magnetorheological (MR) fluids have been used in clutch-type devices for realizing compliant actuation [30–34]. MR clutches have fast response, low nonlinearity, good dynamic performance, and intrinsic compliance. Because of their desirable properties, MR clutches have been used in other high-performance devices such as haptic systems,

rehabilitation equipment, vibration isolation, etc. [35–39]. In most studies, irrespective of the specific application, the mechanical design and manufacturing issues of MR fluid-based devices have been the main focus of research.

In this paper, we provide an in-depth analytical study of the behavior of MR actuators in antagonistic configuration and demonstrate the inherent boundedness of the actuator's output, regardless of the actuator's inputs (both electrical and mechanical inputs). To the best of our knowledge, this is the first study on such properties of MR actuators.

3. Antagonistic Actuation Formalism

In this section, we provide the necessary formulations of antagonistic actuation using MR actuators.

3.1. Magnetorheological Clutch

A magnetorheological (MR) clutch is a rotary device that can control its transmitted torque by varying the viscosity (shear stress) of magnetorheological fluid in response to a magnetic field [40]. The fluid fills the space between input and output disks interleaved with one another in a disk-type MR clutch. We refer to the combination of an active source (such as a DC motor) and an MR clutch as an MR actuator.

An example of an MR clutch is shown in Figure 2. The figure includes the cross-section of a disk-type MR clutch (left) and a snapshot of a prototype MR clutch (right).

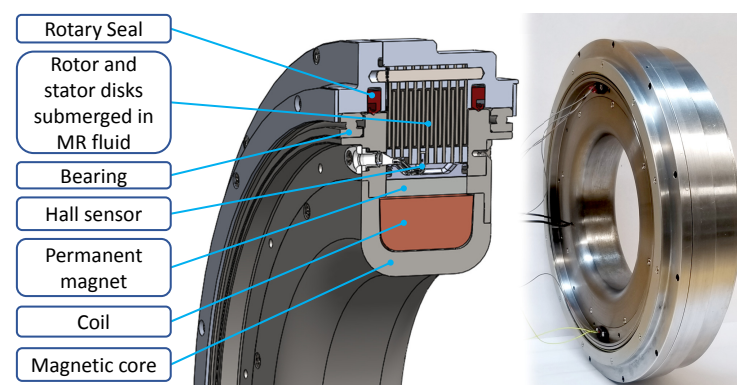


Figure 2. Multi-disk high-torque MR clutch.

The transmitted torque through an MR clutch and the equivalent output torque of an MR actuator can be best described using the Bingham viscoplastic model [41]. For a comprehensive formulation and derivation of the transmission torque of an MR clutch, the readers are referred to [2,42].

3.2. Antagonistic Actuation Using a Pair of MR Clutches

In an antagonistic configuration, two MR clutches drive a single load. The MR clutches receive opposite rotations as their inputs. The opposite rotation is achieved using a single active drive, such as an electric motor, coupled with a transmission mechanism like miter gears. As a result, the MR clutches can transmit the torque to the load both in CW and CCW directions with controllable direction and magnitude. The antagonistic configuration allows driving multiple antagonistic MR clutch pairs using the same active source. Each pair of MR clutches can transmit torque to the corresponding load, enabling independent actuation. Figure 1 illustrates this concept where a single motor drives multiple loads through MR clutches.

Figure 3 shows the CAD model and a snapshot of a prototype 5-DOF collaborative robot developed using this actuation concept. Power transmission between a single DC motor and the five pairs of antagonistic MR clutches is achieved using a combination of belts and shafts. To the best of our knowledge, this is the first 5-DOF robot developed using

the MR actuation concept. For a comprehensive understanding of the complete design, including the robot, actuators, and transmission, we refer interested readers to [43].

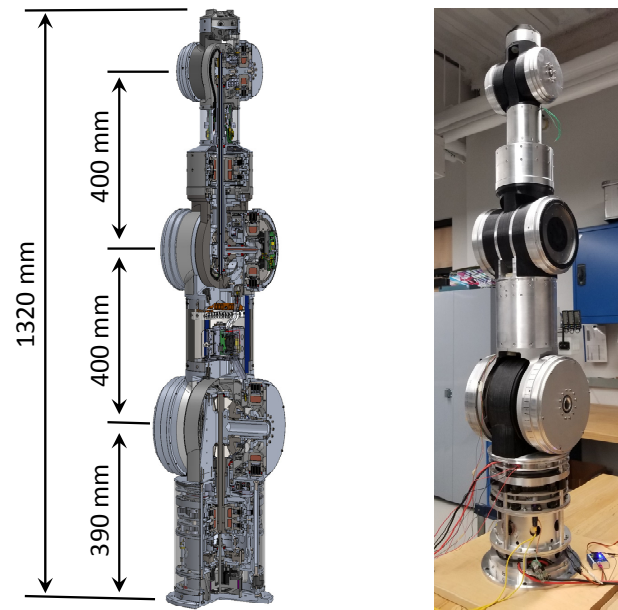


Figure 3. CAD model of internal transmission and photo of a prototype 5-DOF collaborative robot with a single DC motor at the base and 5 pairs of antagonistic MR clutches.

3.3. Torque Formulation of Antagonistic Actuation

The transmission torque of a single MR clutch T_c is often modeled using Bingham plastic models [2]. The magnitude of the transmission torque depends on the applied magnetic field and its direction depends on the relative angular velocity between the input and output of the MR clutch as follows:

$$T_c = T_m(B)\text{sgn}(\Delta\dot{q}) + k_b(\Delta\dot{q}), \quad (1)$$

where $T_m(B)$ is the magnetic-field-dependent positive torque, $\Delta\dot{q}$ is the relative angular velocity between the input and output disks of the MR clutch, and the $\text{sgn}(\cdot)$ function determines the direction of the MR clutch transmission (output) torque with respect to $\Delta\dot{q}$. The $k_b > 0$ is the damping coefficient that accounts for the ever-present viscosity of the MR fluid. To simplify the following formulations, we drop the B and recall that T_m has a positive value. By expanding $\Delta\dot{q}$ as the difference between the MR clutch **input** and **output** velocities, i.e., $\dot{q}_{\text{in}} - \dot{q}$, (1) can be re-written as follows:

$$T_c = T_m \text{sgn}(\dot{q}_{\text{in}} - \dot{q}) + k_b(\dot{q}_{\text{in}} - \dot{q}). \quad (2)$$

From (2), it is clear that the output torque of an MR clutch is always in the direction of the input rotation as long as the MR clutch output (aka stator) rotates slower than its input (aka rotor) in the respective direction, i.e., $|\dot{q}| < |\dot{q}_{\text{in}}|$. We call this an “active” state. On the other hand, if the MR clutch output rotates faster than its input, i.e., $|\dot{q}| > |\dot{q}_{\text{in}}|$, then the direction of output torque is reversed. This switching happens automatically and is inherent in the MR clutch behavior. This behavior is similar to an engine brake in a car friving downhill. We call this the “braking” state.

Finally, if the output of the MR clutch rotates at the same speed as the input, i.e., $|\dot{q}| = |\dot{q}_{\text{in}}|$, the torque transmitted through the MR clutch is assumed to have any value within the $[-T_m, T_m]$ interval. We call this the “transition” state.

In an antagonistic configuration with a pair of MR clutches, the applied torque to the load, T_a can be expressed as the sum of the transmission torque of each MR clutch, i.e.,

$$\begin{aligned}
 T_a &= T_c^+ + T_c^- \\
 &= T_m^+ \text{sgn}(\dot{q}_{in}^+ - \dot{q}) + T_m^- \text{sgn}(\dot{q}_{in}^- - \dot{q}) \\
 &\quad + k_b^+(\dot{q}_{in}^+ - \dot{q}) + k_b^-(\dot{q}_{in}^- - \dot{q}),
 \end{aligned}
 \tag{3}$$

where we use the + and – superscripts to refer to all variables associated with CCW (counterclockwise or positive) and CW (clockwise or negative) directions, respectively. As such, T_m^+ and T_m^- are the magnetic-field-dependent torque of the positive (CCW) and negative (CW) MR clutch, and \dot{q}_{in}^+ and \dot{q}_{in}^- are the respective input velocities.

3.4. Actuator Torque and Joint Velocity Relation

In this section, the relationship between the actuator torque and output velocity (joint velocity) of an antagonistic pair of MR clutches is visually presented. This includes the active, braking, and transition states. For simplicity, we start with an ideal torque–velocity relationship when only the shear stress of the MR fluid is considered while the effects of MR fluid viscosity and the backlash on torque transmission are ignored. Figure 4 depicts the torque–velocity relationship for positive (CCW) and negative (CW) MR clutches and their antagonistic torque.

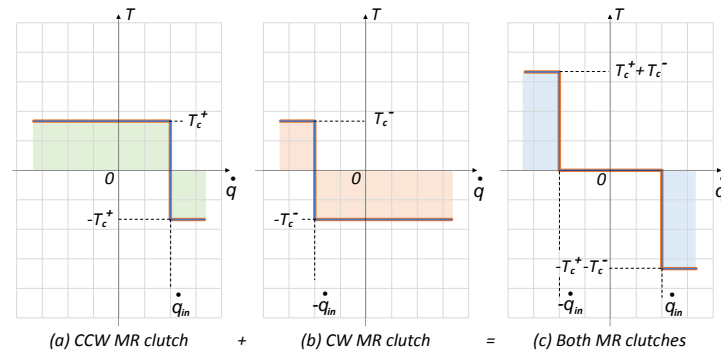


Figure 4. Transmitted torque vs joint angular velocity in an ideal case with $T_c^+ = T_c^-$, and no viscosity or backlash.

It is assumed (due to using a permanent mechanical transmission) that $\dot{q}_{in}^+ = \dot{q}_{in}$, $\dot{q}_{in}^- = -\dot{q}_{in}$ and $\dot{q}_{in} > 0$. Figure 4a shows the switching of the output torque of the positive (CCW) MR clutch from T_c^+ to $-T_c^+$ (active state to braking state) when \dot{q} surpasses \dot{q}_{in} . Figure 4b shows the same behavior for a negative (CW) MR clutch when \dot{q} surpasses $-\dot{q}_{in}$ in the negative direction (i.e., going from $-T_c^-$ to T_c^-). Figure 4c shows the sum of two torques as the antagonistic output. Assuming $T_c^+ = T_c^-$, the output torque is zero when the CCW and CW MR clutches are in their active states ($-\dot{q}_{in} < \dot{q} < \dot{q}_{in}$). Outside the active region, the out torques of MR clutches ally, meaning that the antagonistic torque resists the motion (to exit the braking state) twice as hard.

In practice, one MR clutch of the antagonistic pair is activated, depending on the desired direction. The other MR clutch exerts zero or a small torque due to its friction and remanence. Figure 5a,b depict a case where the positive (CCW) MR clutch is activated to apply the T_c^+ torque. The negative (CW) MR clutch acts as an impediment with a torque $\pm T_c^-$ where $T_c^+ \gg T_c^-$. The antagonistic torque is shown in Figure 5c. The main difference, in this case, is that when both MR clutches are in the active state, the torque is non-zero.

If the effects of MR fluid viscosity, as well as gradual variations in the yield stress [44], are included in the torque–velocity curves of the actuator, the results will be as shown in Figure 6.

The horizontal slopes of the torque–velocity curve reflect the torque increase due to the viscosity of the MR fluid, and the smooth corners of the graph are due to gradual variation of the yield stress [44]. In obtaining these results, it was assumed that the positive (CCW) MR clutch was activated and the other MR clutch exerted a small torque due to its remnant magnetic field and the Coulomb friction in the rotary seals.

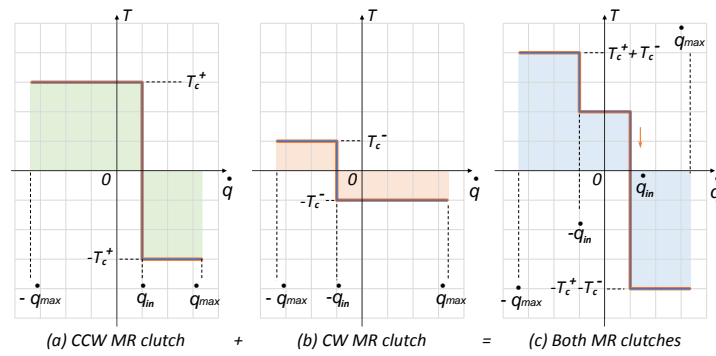


Figure 5. Transmitted torque vs joint angular velocity in an ideal case with $T_c^+ \gg T_c^-$, and no viscosity or backlash.

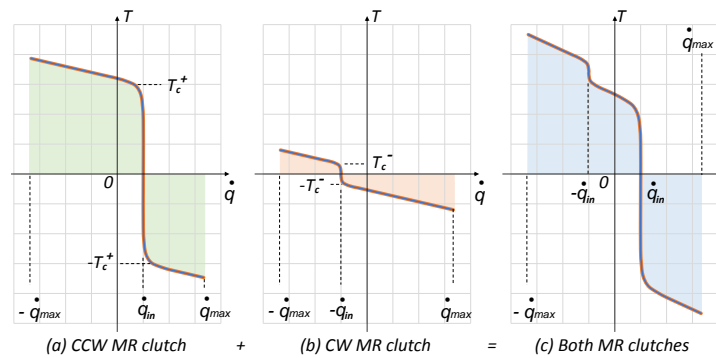


Figure 6. Transmitted torque vs joint angular velocity with $T_c^+ \gg T_c^-$, and MR fluid viscosity is taken into account.

Finally, taking into account the effect of backlash in the mechanical transmission, the torque–velocity curves are updated as shown in Figure 7.

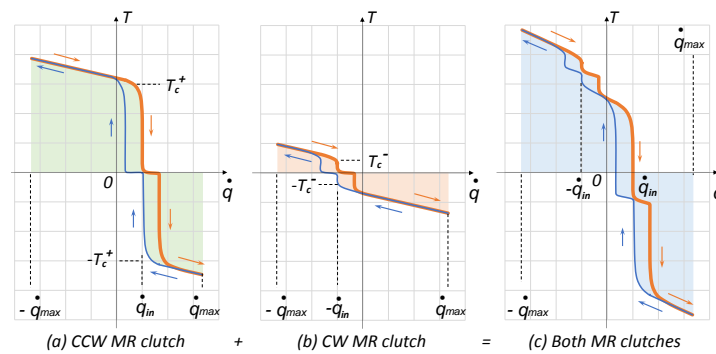


Figure 7. Transmitted torque vs joint angular velocity with $T_c^+ \gg T_c^-$, and MR fluid viscosity and backlash are taken into account.

As observed, the effect of backlash only appears in the results when \dot{q} surpasses \dot{q}_{in} or $-\dot{q}_{in}$ in positive and negative directions, respectively. The backlash is due to the imperfect coupling of mechanical parts. In an MR clutch, this effect appears when momentary decoupling (separation) between the input and output disks inhibits torque transmission as observed in Figure 7.

4. Safe Actuation Relying on Bounded Velocity

The inherent behavior of an MR clutch to switch the direction of the applied torque is unique since it leads to inherent boundedness of the MR actuator output velocity. We know that velocity is an important metric for gauging safe operation as defined in safety standards. The ISO 10218-1:2011 standard specifically limits the maximum speeds of

industrial robots as a requirement for guaranteeing safe operation [45]. In this section, we analyze the behavior of an MR actuator and mathematically prove why the velocity of the MR actuator remains bounded in the entire operational mode. The results are important as they verify the global boundedness of an antagonistic MR actuator, regardless of the control actions on the input current (or magnetic field) and the effect of external forces from interactions with the environment (e.g., humans).

4.1. Uniform Ultimate Velocity Boundedness

Let us consider the dynamics of a single joint robot actuated with an antagonistic pair of MR actuators as follows:

$$J\ddot{q} + k_d\dot{q} + g(q) = T_a, \tag{4}$$

where $J > 0$ is the inertia of the joint, $k_d > 0$ is the damping coefficient of the joint, $g(q)$ is the gravity term, and T_a is the antagonistic torque obtained in (3). Without losing generality, let us assume that we can estimate the gravity forces with some errors ($\tilde{g}(q)$). We also assume that both MR clutches in the pair have similar (but not the same) viscous coefficients since they are manufactured similarly (i.e., $k_b^+ \simeq k_b^-$). Under these assumptions, we can re-write (4) after substituting T_a with its value from (3) as follows:

$$J\ddot{q} + k_d\dot{q} = T_m^+(t) \operatorname{sgn}(\dot{q}_{in} - \dot{q}) + T_m^-(t) \operatorname{sgn}(-\dot{q}_{in} - \dot{q}) - 2k_b\dot{q} + \delta(t), \tag{5}$$

where all parameters are as defined previously and $\delta(t)$ is a Lebesgue locally essential bounded function of time which represents disturbances that account for any estimation error in gravity forces, i.e., $\tilde{g}(q) - g(q)$, and any mismatch of the viscous coefficients between MR clutches, i.e., $(k_b^+ - k_b^-)\dot{q}_{in}$. It is also assumed that $T_m^+(t)$ and $T_m^-(t)$ are Lebesgue measurable functions of time, $t, \dot{q}_{in} > 0$, and $k_b \geq 0$ are constants. Under these assumptions, the following results are valid.

Proposition 1. Consider System (5), where $\max\{k_b, k_d\} > 0$. Then, for any $t_0 \geq 0$, and any initial condition $\dot{q}(t_0) \in (-\infty, \infty)$, the following inequality,

$$|\dot{q}(t)| \leq \max \left\{ |\dot{q}(t_0)| e^{-\frac{1}{2}k_0(t-t_0)}, \dot{q}_{in}, \sup_{\tau \in [t_0, t]} \frac{2(\delta(\tau) - T_m^+(\tau) - T_m^-(\tau))}{2k_b + k_d} \right\}, \tag{6}$$

will hold along all trajectories of System (5) for all $t \geq t_0$, where $k_0 \triangleq \frac{1}{J}(2k_b + k_d) > 0$.

For simplicity, let us not explicitly show the dependency of \dot{q} , T_m^+ , T_m^- and δ to time and drop t .

Proof. Consider an ISS (input-to-state stability) Lyapunov function candidate,

$$V(\dot{q}) = \frac{1}{2}J\dot{q}^2, \tag{7}$$

where $V(\dot{q})$ is positive definite. The time derivative of $V(\dot{q})$ along the trajectories of (5) is given by

$$\begin{aligned} \dot{V} &= \dot{q}J\ddot{q} = \dot{q}(-k_d\dot{q} + T_m^+ \operatorname{sgn}(\dot{q}_{in} - \dot{q}) + T_m^- \operatorname{sgn}(-\dot{q}_{in} - \dot{q}) - 2k_b\dot{q} + \delta(t)) \\ &= T_m^+ \operatorname{sgn}(\dot{q}_{in} - \dot{q})\dot{q} + T_m^- \operatorname{sgn}(-\dot{q}_{in} - \dot{q})\dot{q} - (2k_b + k_d)\dot{q}^2 + \dot{q}\delta. \end{aligned} \tag{8}$$

Suppose $|\dot{q}| > \dot{q}_{in}$, equivalently, $V > V_{in} \triangleq \frac{1}{2}J\dot{q}_{in}^2$. In this case, $\text{sgn}(\dot{q}_{in} - \dot{q}) = \text{sgn}(-\dot{q}) = -\text{sgn}(\dot{q})$, and, similarly, $\text{sgn}(-\dot{q}_{in} - \dot{q}) = \text{sgn}(-\dot{q}) = -\text{sgn}(\dot{q})$. Therefore, assuming $|\dot{q}| > \dot{q}_{in}$, (8) implies

$$\begin{aligned} \dot{V} &= - (T_m^+ + T_m^-)|\dot{q}| - (2k_b + k_d)|\dot{q}|^2 + \dot{q}\delta \leq \\ &\quad - (2k_b + k_d)|\dot{q}|^2 + (\delta - (T_m^+ + T_m^-))|\dot{q}| \leq \\ &\quad - \frac{2k_b + k_d}{2}|\dot{q}|^2 \\ &\quad - \left(\frac{2k_b + k_d}{2}|\dot{q}| - (\delta - (T_m^+ + T_m^-)) \right)|\dot{q}| \leq \\ &\quad - k_0V - \left(\frac{2k_b + k_d}{2}|\dot{q}| - (\delta - (T_m^+ + T_m^-)) \right)|\dot{q}|. \end{aligned} \tag{9}$$

We see that

$$\dot{V} < -k_0V \tag{10}$$

whenever

$$|\dot{q}| > \max\left\{\dot{q}_{in}, \frac{2(\delta - T_m^+ - T_m^-)}{2k_b + k_d}\right\}.$$

The statement of Proposition 1 now follows by application of the comparison principle and ISS type arguments (see Sections 3.4 and 4.9 in [46]). □

Proposition 1 implies that the velocity of an MR actuator is uniformly ultimately bounded for any uniformly essentially bounded disturbance $\delta(t)$. If $\delta(t) \leq T_m^+(t) + T_m^-(t)$ for (almost) all $t \geq 0$, then the set $|\dot{q}(t)| \leq \dot{q}_{in}$ is forward invariant, i.e., $|\dot{q}(t_0)| \leq \dot{q}_{in}$ implies $|\dot{q}(t)| \leq \dot{q}_{in}$ for all $t \geq t_0$.

These results are important as they show that the system velocity remains within a bound regardless of what the control commands to an antagonistic MR actuator are or what conditions are imposed by the external environment.

4.2. Safe Control Design

The antagonistic MR actuator provides new possibilities for designing control algorithms that are geared toward safety. We describe one example of a control algorithm using the model given in (5) and experimentally validate the performance of this algorithm.

We know that the severity of an accident (e.g., collision) with a robot manipulator directly relates to the energy transferred from the robot to the human [45]. Thus, one common strategy in designing a human-safe robot is to limit the total kinetic energy of the system to a safe limit. We also know that an antagonistic MR actuator (as shown in the previous section) limits the output velocity of the actuator in the entire operation mode. These two facts allow for designing control strategies that are specifically tailored for human-safe operations. In other words, we can design control algorithms for MR actuators that guarantee an upper limit for the kinetic energy delivered by the robot.

To demonstrate this, let us assume an upper bound for the total kinetic energy of the system, λ_{max} , for which we can guarantee the safety of the human in case of an accident. Considering the total kinetic energy of the system defined in (5) along all system trajectories as

$$E_k(\dot{q}) = \frac{1}{2}J\dot{q}^2, \tag{11}$$

the objective of the safe control design is to limit the kinetic energy as follows:

$$E_k(\dot{q}) \leq \lambda_{max}, \quad \forall \dot{q} \in \mathbb{R}. \tag{12}$$

We consider a gear ratio of β between the motor and the input (rotor) of the MR clutches, i.e.,

$$\dot{q}_{in} = \beta\dot{q}_{mot}, \tag{13}$$

where \dot{q}_{mot} is the velocity of the motor. We previously showed that the joint velocity of the system was uniformly ultimately bounded to $|\dot{q}_{\text{in}}|$. Using these results, it can be shown that

$$\frac{1}{2}J\dot{q}^2 \leq \frac{1}{2}J\dot{q}_{\text{in}}^2 \leq \frac{1}{2}J(\beta\dot{q}_{\text{mot}})^2. \quad (14)$$

To satisfy the safe control design requirement defined in (12), there exists an explicit solution for the motor velocity that guarantees total kinetic energy along all system trajectories, i.e.,

$$\dot{q}_{\text{mot}} \leq \left(\frac{2\lambda_{\text{max}}}{J\beta^2}\right)^{\frac{1}{2}}. \quad (15)$$

The limit set on the velocity acts on top of any other control action, allowing the robot the performance of any desired operations. Since the motor is mechanically decoupled from the load, it is guaranteed that the antagonistic MR actuation will not deliver more kinetic energy to the system than the safe level along any system trajectory. This statement is true even when the load is driven externally such that the total kinetic energy of the system exceeds the safe level by external factors, in which case the automatic switching of the actuator to the braking mode will resist joint velocity until the kinetic energy of the system returns to the safe level (unless the external forces exceed the MR actuator capabilities). One should note that this behavior is inherent to the actuator and does not depend on any sensor measurements or any specific control algorithm.

Similar control strategies based on deliverable torque or stiffness control can be achieved using antagonistic MR actuators with the same level of simplicity and intuitiveness. We leave comprehensive discussions related to control design and the extension of the results to multi-DOF mechanisms to future publications.

In the next section, we provide experimental results to validate the theories discussed in this section.

5. Experimental Result

In this section, experimental results validating our previous analyses are presented. The first experiment demonstrates the relationship between the transmitted torque and angular velocity of a pair of antagonistic MR clutches, confirming the braking behavior described in Figure 7. The second experiment implements and assesses the performance of the control strategy for limiting the kinetic energy of a specific system.

The experiments are conducted using the second joint of the 5-DOF manipulator in the configuration depicted in Figure 8. Similar results could be obtained from other joints, as they are actuated similarly. Such results are not included to maintain brevity.

The experimental setup used to obtain the results in this section is illustrated in Figure 9. The setup comprises a load cell (force/torque sensor ATI Gamma US-15-50) installed between the second link and the KUKA LWR 4+ robot flange to measure Joint 2 torque. Besides the MR clutch torque, the force/torque sensor readings contain other components, such as friction, inertial, and gravity forces. To minimize the impact of some (but not all) of these undesired components on the sensor measurements, the upper joints of the robot are removed during the experiments. Moreover, to improve the accuracy of the sensor readings, the gravity and inertial forces are computationally estimated and considered in subsequent calculations. The effect of gravity and inertial forces on the results are discussed and demonstrated later in this section.

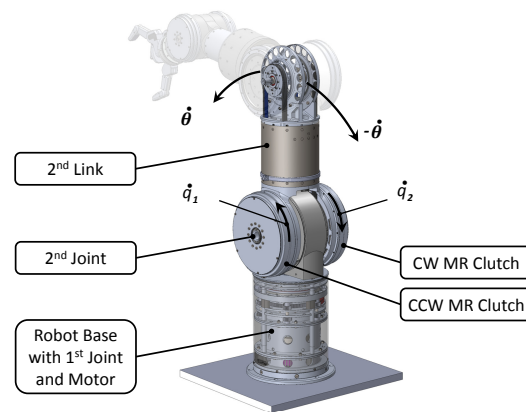


Figure 8. Second joint of the 5-DOF manipulator used as an antagonistic MR-clutch pair experimental setup.

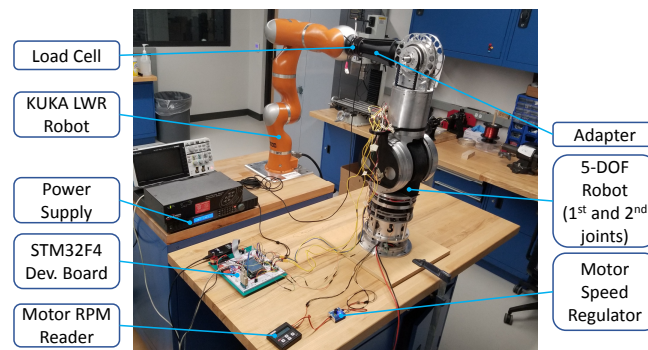


Figure 9. Experimental set up consisting of a KUKA LWR 4+ robot coupled to the second link of the MR actuated 5-DOF robot.

Joint 2 (as well as each joint of the 5-DOF manipulator) is equipped with an Absolute 17-bit encoder from Zettlex to measure the angular position and velocity of the corresponding joint at a frequency of 10 kHz. Current control for each MR clutch is performed using the STM32F407VET6 microcontroller and a pair of H-bridge current drivers, TI DRV8874. The experimental data acquisition is performed using the same STM32F407VET6 microcontroller with measurements conducted at a sampling frequency of 1 kHz.

The 5-DOF robot is actuated by a single brushless DC motor (Hacker, model Q80-13XS F3A) with a harmonic gearbox (SHD-25-100-2SH). The motor and gearbox are positioned at the base of the robot which minimizes the moving inertia of the system.

5.1. Torque–Velocity Relationship

To obtain the relationship between the transmitted torque of an antagonistic MR clutch pair and its output velocity, the positive (CCW) and negative (CW) MR clutches in Joint 2 of the (modified) 5-DOF manipulator were used. During the experiment, joint 2 of the manipulator was moved externally by the KUKA robot back and forth, while one of the MR clutches in the pair was activated with a constant current. The sequence of robot poses representing the reciprocal motion of Joint 2 is shown in Figure 10.

The external motion was selected in such a way that it forced the activated MR clutch into both active and braking states. To achieve this, the joint was moved by the external source so that the output velocity of the MR clutch (i.e., the joint velocity) during some areas of the movement exceeded its input velocity, i.e., $|\dot{q}| > \dot{q}_{in}$.

The KUKA LWR 4+ robot attached to the second joint was used to move the joint within the ± 20 degree range from its upright position. At the same time, the positive (CCW) MR clutch was energized with a constant current of 0.2 A (corresponding to 15 N·m). The negative (CW) MR clutch was not activated. The input (rotor) velocity of the positive (CCW) MR clutch was set to 6 deg/s. Joint 2 was moved to reach a velocity of ± 40 deg/s

during its motion. A similar experiment was repeated using the negative (CW) MR clutch. The results from these experiments are shown in Figure 11.

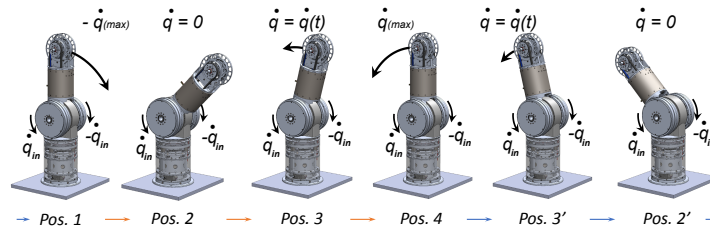


Figure 10. Sequence of the reciprocating motions of the second joint of the robot. A KUKA LWR4+ robot coupled with Joint 2 of the modified manipulator was commanded to follow a sinusoidal trajectory in position-controlled mode, resulting in the reciprocating motions of Joint 2.

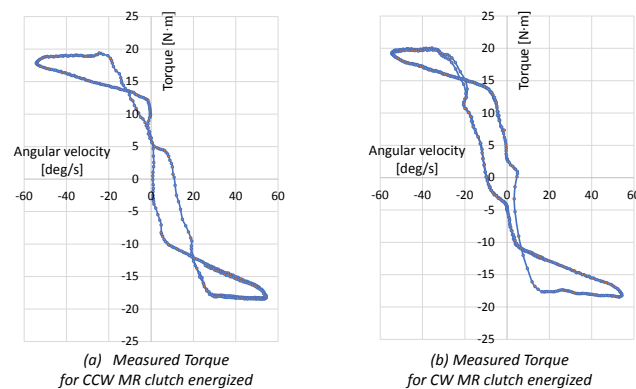


Figure 11. Torque–Velocity curves of antagonistic MR clutches in the second joint, with the output torque set to ± 15 N·m (0.2 A) and the input velocity set to ± 6 deg/s.

It is observed that the direction of the MR clutch output torque depends on the relative velocity between its input and output. This behavior was previously described and modeled in Sections 3.3 and 3.4, respectively. In our experiment, the output torque of the MR clutches in the pair was set to ± 15 N·m, and their input velocity was set to ± 6 deg/s. One can clearly see the transition of the positive (CCW) MR clutch torque from 15 N·m to -15 N·m once its output velocity surpasses 6 deg/s. The opposite behavior is also seen for negative (CW) MR clutch below -6 deg/s.

The torque–velocity curves appear with visible distortions in both regions. The distortions are due to the effect of gravity, friction, inertia (of Link 2), and structural flexibility on the measurements. The distortions in the low–velocity region of the curves are mostly due to the limited rigidity of the structure and the backlash in the mechanical transmission, both of which are difficult to model accurately. On the other hand, the distortions in the high–velocity region are mostly due to the inertial and gravitational forces which can be modeled with relatively good accuracy using the joint angle measurements and the known values of the robot masses. We estimated the inertial and gravity forces and subtracted these values from force/torque measurements. The corrected torque–velocity curves for both MR clutches after removing the effects of the inertial and gravity forces are shown in Figure 12.

As seen, the torque–velocity curves more closely represent the relationship described in Section 3.4. A comparison of the experimental torque–velocity curve of the positive (CCW) MR clutch with that obtained theoretically is shown in Figure 13 and further validates the results.

As observed, there is a good match between the two curves at high–velocity regions where the effects of inertia and gravity forces were removed from the graph. The main mismatch between the two curves occurs in low–velocity regions where it is difficult to

accurately model the effect of backlash and structural flexibility on the curves. Nonetheless, the results validate our modeling approach of the behavior of the antagonistic MR actuators.

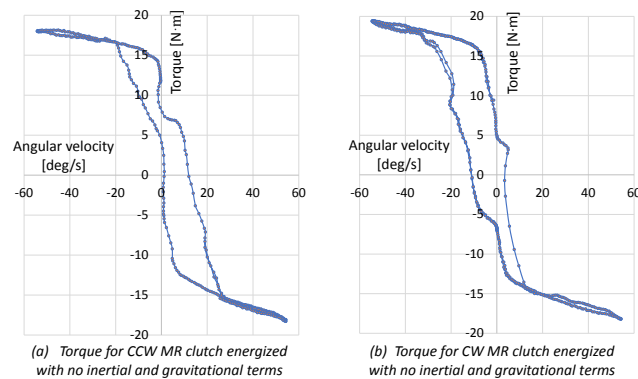


Figure 12. Torque–velocity curves of antagonistic MR clutches in the second joint with inertial and gravitational forces removed, the output torque set to ± 15 N·m (0.2 A), the input velocity set to ± 6 deg/s.

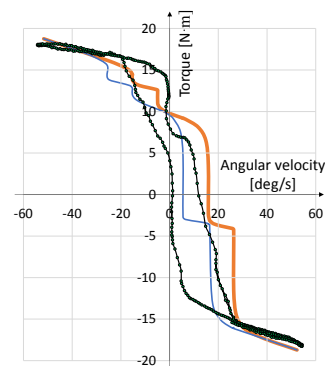


Figure 13. Comparison of the experimental and theoretical torque–velocity curves of the antagonistic MR clutches in the second joint of the robot manipulator.

5.2. Safe Control Strategy

In this section, we study the performance of the safe control strategy described in Section 4.2. We selected an upper limit of 10 mJ for the kinetic energy of the robot. This value was arbitrarily selected for the purpose of demonstration only and has no significance. By using this value in (15), an upper limit velocity for the motor was obtained to be 50 RPM. The motor velocity resulted in an input velocity of ± 6 deg/s for the positive and negative MR clutches in the second joint. The MR clutches in this joint were energized to move the robot link in a reciprocal motion with a constant velocity of ± 3.5 deg/s, similar to the motion shown in Figure 10.

The difference with the previous experiment is that the robot motion is generated by its own actuators, i.e., the robot's motor and its antagonistic MR clutches, rather than an external source (KUKA manipulator).

The KUKA LWR 4+ manipulator attached to the second link is used to introduce random external disturbances during the motion of the second joint. This enabled us to evaluate the performance of the controller for limiting the kinetic energy of the system through the inherent switching of MR clutches to the braking state. The KUKA robot moves along Link 2 trajectory in a compliant mode except that from time to time it exerts a disturbance torque that results in the second joint moving at a speed above the upper limit set by the controller (i.e., ± 6 deg/s). The higher speed violated the limit for kinetic energy in the system permitted by the controller.

The results of this experiment are shown in Figure 14. The figure includes the angular position and angular velocity of the second joint, the antagonistic torque of the MR clutch pair, and the total kinetic energy of the system.

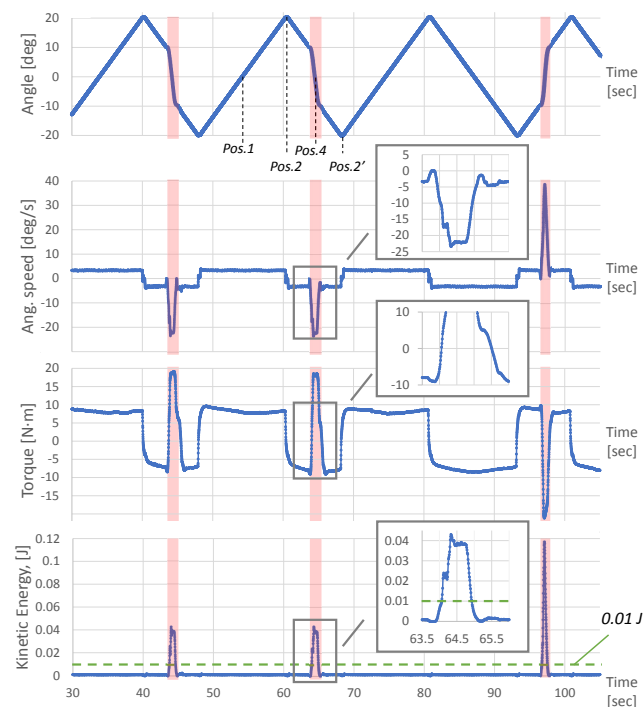


Figure 14. Inherent behavior of antagonistic MR clutches pair in response to external disturbances.

The figure shows the expected motion of the joint as well as three different random perturbations caused by the KUKA robot. As seen, two perturbations (around 45 and 65 s) occurred during the clockwise rotation and forced the angular velocity of the joint from -6 deg/s to -24 deg/s momentarily. The third perturbation (around 95 s) occurred during the counter-clockwise rotation, forcing the velocity of the joint from 6 deg/s to about 39 deg/s momentarily.

Looking at the Kinetic energy graph, one can see that as soon as the velocity of either MR clutches surpasses the ± 6 deg/s limits, the system kinetic energy crosses the 10 mJ threshold. This causes an immediate control reaction by instantaneous reversal of the direction of the applied torque by the corresponding MR clutch which subsequently forces the system to return to the active region by resisting the KUKA robot. Through this action, the controller limits the kinetic energy of the system to the desired value by reducing the output velocity below the set value. The braking states in the figure are marked with a red color background to highlight this inherent behavior. To better demonstrate the order in which the system responds to a kinetic energy limit violation, a small portion of the velocity, torque, and kinetic energy graphs are magnified. By looking at the exact time, it is observed that the increase in the velocity and kinetic energy is followed by the reversal of the torque direction.

The importance of these results is that the observed behavior occurs inherently, without relying on any sensor measurements, and is also independent of the state of the low-level control algorithm commanding the robot with MR actuators to follow the trajectory. The response is triggered as soon as the kinetic energy in the system, or equivalently the joint velocity, exceeds a predetermined threshold, at which point the corresponding MR clutch immediately acts as a brake with a torque that opposes the motion. The results clearly validate the uniform ultimate velocity boundedness of the MR actuation.

The results can be extended to multi-DOF actuation. However, it is beyond the scope of the current paper to describe its details and will be studied in future work.

6. Conclusions

In this paper, we presented a theoretical and experimental study on the intrinsic behavior of antagonistic Magneto-Rheological (MR) clutches.

The natural behavior of antagonistic MR clutches in bounding the output velocity was carefully examined. The study demonstrated the uniform ultimate boundedness of the velocity of antagonistic MR actuators in the presence of external disturbances. A graphical representation illustrating this behavior was provided, and the effects of undesired nonlinearities, such as mechanical backlash, yield stress variations, and viscosity of the MR fluid, were analyzed.

The theoretical findings were experimentally validated using a setup comprising a pair of antagonistic MR clutches in the second joint of a 5-DOF compliant robot and a KUKA LWR 4+ robot. The experiments confirmed that antagonistic MR actuators actively resist external sources and exhibit an inherent tendency to maintain an active state while limiting the output velocity.

Notably, the study's broader implications support our earlier claims regarding the suitability of MR actuation for safe, intuitive, and reliable actuation, without the complexities and high costs associated with alternative approaches. The results highlight the suitability of MR actuators and demonstrate the potential for designing systems that exhibit safe and reliable behavior throughout the control region, without compromising actuation performance or incurring excessive design costs.

Author Contributions: Conceptualization, M.R.K. and S.P.; methodology, M.R.K., S.P., Z.-Q.Y.; software, S.P. and Z.-Q.Y.; validation, M.R.K. and S.P.; formal analysis, M.R.K., I.P. and S. Piestskiy; investigation, M.R.K. and S.P.; resources, M.R.K.; data curation, S.P. and M.R.K.; writing—original draft preparation, M.R.K.; writing—review and editing, M.R.K.; visualization, S.P., Z.-Q.Y.; supervision, M.R.K.; project administration, M.R.K.; funding acquisition, M.R.K. All authors have read and agreed to the published version of the manuscript.

Funding: The authors acknowledge the support from the Canada Foundation for Innovation (CFI) and Natural Sciences and Engineering Research Council (NSERC) of Canada under grant reference numbers: 25031 and RGPIN-346166.

Data Availability Statement: Not applicable.

Conflicts of Interest: The authors declare no conflict of interest.

References

1. Tesla Shows Walking Optimus Robot at Investor Day. Available online: <https://www.youtube.com/watch?v=voqAQtpWiHs> (accessed on 2 August 2023).
2. Shafer, A.S.; Kermani, M.R. On the feasibility and suitability of MR fluid clutches in human-friendly manipulators. *IEEE/ASME Trans. Mechatron.* **2011**, *16*, 1073–1082. [CrossRef]
3. Lucidarme, P.; Delanoue, N.; Mercier, F.; Aoustin, Y.; Chevallereau, C.; Wenger, P. Preliminary Survey of Backdrivable Linear Actuators for Humanoid Robots. In Proceedings of the ROMANSY 22—Robot Design, Dynamics and Control, CISM International Centre for Mechanical Sciences, Rennes, France, 25–28 June 2018; Springer: Berlin/Heidelberg, Germany, 2019; Volume 584.
4. Haddadin, S.; Parusel, S.; Johannsmeier, L.; Golz, S.; Gabl, S.; Walch, F.; Sabaghian, M.; Jähne, C.; Hausperger, L.; Haddadin, S. The franka emika robot: A reference platform for robotics research and education. *IEEE Robot. Autom. Mag.* **2022**, *29*, 46–64. [CrossRef]
5. Ionescu, T.B. Adaptive simplex architecture for safe, real-time robot path planning. *Sensors* **2021**, *21*, 2589. [CrossRef]
6. Maheu, V.; Archambault, P.S.; Frappier, J.; Routhier, F. Evaluation of the JACO robotic arm: Clinico-economic study for powered wheelchair users with upper-extremity disabilities. In Proceedings of the 2011 IEEE International Conference on Rehabilitation Robotics, Zurich, Switzerland, 29 June–1 July 2011; pp. 1–5.
7. Abdeetedal, M.; Kermani, M.R. An open-source integration platform for multiple peripheral modules with Kuka robots. *CIRP J. Manuf. Sci. Technol.* **2019**, *27*, 46–55. [CrossRef]
8. Nicolis, D.; Allevi, F.; Rocco, P. Operational space model predictive sliding mode control for redundant manipulators. *IEEE Trans. Robot.* **2020**, *36*, 1348–1355. [CrossRef]
9. The New Sawyer BLACK Edition. Brochure. Available online: https://www.rethinkrobotics.com/fileadmin/user_upload/sawyer/rr-blackedition-brochure_low.pdf (accessed on 2 August 2023).
10. Cremer, S.; Mastromoro, L.; Popa, D.O. On the performance of the Baxter research robot. In Proceedings of the 2016 IEEE International Symposium on Assembly and Manufacturing (ISAM), Fort Worth, TX, USA, 21–22 August 2016; pp. 106–111.
11. Yadmellat, P.; Kermani, M.R. Adaptive modeling of a fully hysteretic magneto-rheological clutch. In Proceedings of the 2012 IEEE International Conference on Robotics and Automation (ICRA), Saint Paul, MI, USA, 14–18 May 2012; pp. 2698–2703.

12. Pisetskiy, S.; Kermani, M.R. High-performance magneto-rheological clutches for direct-drive actuation: Design and development. *J. Intell. Mater. Syst. Struct.* **2021**, *32*, 2582–2600. [[CrossRef](#)]
13. *ISO/TS 15066; Robots and Robotic Devices—Collaborative Robots*. ISO: Geneva, Switzerland, 2016.
14. Althoefer, K. Antagonistic actuation and stiffness control in soft inflatable robots. *Nat. Rev. Mater.* **2018**, *3*, 76–77. [[CrossRef](#)]
15. Roozing, W.; Li, Z.; Medrano-Cerda, G.A.; Caldwell, D.G.; Tsagarakis, N.G. Development and Control of a Compliant Asymmetric Antagonistic Actuator for Energy Efficient Mobility. *IEEE/ASME Trans. Mechatron.* **2016**, *21*, 1080–1091. [[CrossRef](#)]
16. Grebenstein, M.; Albu-Schäffer, A.; Bahls, T.; Chalon, M.; Eiberger, O.; Friedl, W.; Gruber, R.; Haddadin, S.; Hagn, U.; Haslinger, R.; et al. The DLR hand arm system. In Proceedings of the IEEE International Conference on Robotics and Automation, Shanghai, China, 9–13 May 2011; pp. 3175–3182.
17. Yip, M.C.; Niemeyer, G. High-performance robotic muscles from conductive nylon sewing thread. In Proceedings of the 2015 IEEE International Conference on Robotics and Automation (ICRA), Seattle, WA, USA, 26–30 May 2015; pp. 2313–2318.
18. Jafarzadeh, M.; Gans, N.; Tadesse, Y. Control of TCP muscles using Takagi–Sugeno–Kang fuzzy inference system. *Mechatronics* **2018**, *53*, 124–139. [[CrossRef](#)]
19. Grant, D.; Hayward, V. Variable structure control of shape memory alloy actuators. *IEEE Control Syst. Mag.* **1997**, *17*, 80–88.
20. Ganguly, S.; Garg, A.; Pasricha, A.; Dwivedy, S. Control of pneumatic artificial muscle system through experimental modelling. *Mechatronics* **2012**, *22*, 1135–1147. [[CrossRef](#)]
21. Pratt, G.; Williamson, M.M. Series elastic actuators. In Proceedings of the 1995 IEEE/R SJ International Conference on Intelligent Robots and Systems 95, ‘Human Robot Interaction and Cooperative Robots’ Proceedings, Pittsburgh, PA, USA, 5–9 August 1995; Volume 1, pp. 399–406.
22. Tonietti, G.; Schiavi, R.; Bicchi, A. Design and control of a variable stiffness actuator for safe and fast physical human/robot interaction. In Proceedings of the 2005 IEEE International Conference on Robotics and Automation ICRA 2005, Barcelona, Spain, 18–22 April 2005; pp. 526–531.
23. Schiavi, R.; Grioli, G.; Sen, S.; Bicchi, A. VSA-II: A novel prototype of variable stiffness actuator for safe and performing robots interacting with humans. In Proceedings of the IEEE International Conference on Robotics and Automation ICRA 2008, Pasadena, CA, USA, 19–23 May 2008; pp. 2171–2176.
24. Chew, C.M.; Hong, G.S.; Zhou, W. Series damper actuator: A novel force/torque control actuator. In Proceedings of the 2004 4th IEEE/RAS International Conference on Humanoid Robots, Santa Monica, CA, USA, 10–12 November 2004; Volume 2, pp. 533–546.
25. Liu, L.; Leonhardt, S.; Misgeld, B.J. Design and control of a mechanical rotary variable impedance actuator. *Mechatronics* **2016**, *39*, 226–236. [[CrossRef](#)]
26. Zinn, M.; Roth, B.; Khatib, O.; Salisbury, J.K. A new actuation approach for human friendly robot design. *Int. J. Robot. Res.* **2004**, *23*, 379–398. [[CrossRef](#)]
27. Wimböck, T.; Ott, C.; Hirzinger, G. Immersion and invariance control for an antagonistic joint with nonlinear mechanical stiffness. In Proceedings of the 49th IEEE Conference on Decision and Control (CDC), Atlanta, GA, USA, 15–17 December 2010; pp. 1128–1135.
28. Mengacci, R.; Garabini, M.; Grioli, G.; Catalano, M.; Bicchi, A. Overcoming the Torque/Stiffness Range Tradeoff in Antagonistic Variable Stiffness Actuators. *IEEE/ASME Trans. Mechatron.* **2021**, *26*, 3186–3197. [[CrossRef](#)]
29. Park, J.; Hong, G.Y.; Choi, Y.; Peng, D.; Lu, Q. Passivity based Control of Antagonistic Tendon-Driven Mechanism. In Proceedings of the 2019 International Conference on Robotics and Automation (ICRA), Montreal, QC, Canada, 20–24 May 2019; pp. 3095–3100.
30. Bégin, M.A.; Denninger, M.; Plante, J.S. Design and Experimental Validation of a 2DOF Sidestick Powered by Hyper-Redundant Magnetorheological Actuators Providing Active Feedback. In Proceedings of the 2019 International Conference on Robotics and Automation (ICRA), Montreal, QC, Canada, 20–24 May 2019; pp. 4011–4017.
31. Li, W.; Yadmellat, P.; Kermani, M.R. Linearized torque actuation using FPGA-controlled magnetorheological actuators. *IEEE/ASME Trans. Mechatron.* **2015**, *20*, 696–704. [[CrossRef](#)]
32. Moghani, M.; Kermani, M.R. Hysteresis modeling of a hybrid magneto-rheological actuator. In Proceedings of the 2016 IEEE International Conference on Advanced Intelligent Mechatronics (AIM), Banff, AB, Canada, 12–15 July 2016; pp. 246–251.
33. Yadmellat, P.; Kermani, M.R. Study of limit cycle in antagonistically coupled magneto-rheological actuators. *Control Eng. Pract.* **2015**, *35*, 92–101. [[CrossRef](#)]
34. Oh, J.S.; Sohn, J.W.; Choi, S.B. Applications of magnetorheological fluid actuator to multi-DOF systems: State-of-the-art from 2015 to 2021. *Actuators* **2022**, *11*, 44. [[CrossRef](#)]
35. Fauteux, P.; Lauria, M.; Heintz, B.; Michaud, F. Dual-differential rheological actuator for high-performance physical robotic interaction. *IEEE Trans. Robot.* **2010**, *26*, 607–618. [[CrossRef](#)]
36. Kikuchi, T.; Takano, T.; Yamaguchi, A.; Ikeda, A.; Abe, I. Haptic interface with twin-driven MR fluid actuator for teleoperation endoscopic surgery system. *Actuators* **2021**, *10*, 245. [[CrossRef](#)]
37. Véronneau, C.; Denis, J.; Lebel, L.P.; Denninger, M.; Blanchard, V.; Girard, A.; Plante, J.S. Multifunctional remotely actuated 3-DOF supernumerary robotic arm based on magnetorheological clutches and hydrostatic transmission lines. *IEEE Robot. Autom. Lett.* **2020**, *5*, 2546–2553. [[CrossRef](#)]
38. Diep, B.T.; Nguyen, N.D.; Tran, T.T.; Nguyen, Q.H. Design and experimental validation of a 3-DOF force feedback system featuring spherical manipulator and magnetorheological actuators. *Actuators* **2020**, *9*, 19. [[CrossRef](#)]

39. Wu, X.; Huang, C.; Tian, Z.; Ji, J. Development of a novel magnetorheological fluids transmission device for high-power applications. *Smart Mater. Struct.* **2019**, *28*, 055021. [[CrossRef](#)]
40. Shafer, A.S.; Kermani, M.R. Design and validation of a magneto-rheological clutch for practical control applications in human-friendly manipulation. In Proceedings of the 2011 IEEE International Conference on Robotics and Automation (ICRA), Shanghai, China, 9–13 May 2011; pp. 4266–4271.
41. Phillips, R.W. Engineering Applications of Fluids with a Variable Yield Stress. Ph.D. Thesis, University of California, Berkeley, CA, USA, 1969.
42. Yang, Z.Q.; Kermani, M.R. A Computationally Efficient Hysteresis Model for Magneto-Rheological Clutches and Its Comparison with Other Models. *Actuators* **2023**, *12*, 190. [[CrossRef](#)]
43. Pisetskiy, S.; Kermani, M.R. Design and Development of the Transmission for a Fully Actuated 5-Degrees-of-Freedom Compliant Robot Manipulator with a Single Motor. *J. Mech. Robot.* **2024**, *16*, 021003. [[CrossRef](#)]
44. Ahmadkhanlou, F.; Mahboob, M.; Bechtel, S.; Washington, G. An improved model for magnetorheological fluid-based actuators and sensors. *J. Intell. Mater. Syst. Struct.* **2010**, *21*, 3–18. [[CrossRef](#)]
45. ISO 10218-1:2011; Robots and Robotic Devices—Safety Requirements for Industrial Robots. ISO. Available online: <https://www.iso.org/obp/ui/#iso:std:iso:10218:-1:ed-2:v1:en> (accessed on 18 July 2023).
46. Khalil, H.K. *Nonlinear Systems*, 3rd ed.; Prentice Hall: Upper Saddle River, NJ, USA, 2002.

Disclaimer/Publisher’s Note: The statements, opinions and data contained in all publications are solely those of the individual author(s) and contributor(s) and not of MDPI and/or the editor(s). MDPI and/or the editor(s) disclaim responsibility for any injury to people or property resulting from any ideas, methods, instructions or products referred to in the content.